JOURNAL OF CHEMICAL INFORMATION AND MODELING

Article

pubs.acs.org/jcim

Theoretical Studies on the Susceptibility of Oseltamivir against Variants of 2009 A/H1N1 Influenza Neuraminidase

Lin Li,[†] Youyong Li,[†] Liling Zhang,[†] and Tingjun Hou*[,†,‡]

[†]Institute of Functional Nano & Soft Materials (FUNSOM) and Jiangsu Key Laboratory for Carbon-Based Functional Materials & Devices, Soochow University, Suzhou, Jiangsu 215123, China

[‡]College of Pharmaceutical Sciences, Soochow University, Suzhou, Jiangsu 215123, China

Supporting Information

ABSTRACT: The outbreak and high speed global spread of the new strain of influenza A/H1N1 virus in 2009 posed a serious threat to global health. It is more likely that drug-resistant influenza strains will arise after the extensive use of anti-influenza drugs. Consequently, the identification of the potential resistant sites for drugs in advance and the understanding of the corresponding molecular mechanisms that cause drug resistance are quite important in the design of new drug candidates with better potency to combat drug resistance. Here, we performed molecular simulations to evaluate the potency of oseltamivir to combat drug resistance caused by the mutations in 2009 A/H1N1 neuraminidase (NA). We examined three representative drug-resistant mutations in NA, consisting of H274Y, N294S, and Y252H. First, a theoretical structure of A/H1N1 NA in complex with oseltamivir was constructed using homology modeling. Then, molecular dynamics (MD) simulations, molecular mechanics/Poisson−Boltzmann surface area (MM/PBSA) calculations, and MM/GBSA free energy decomposition were used to characterize the binding of oseltamivir with the wild type (WT) and three mutated NAs. Our predictions show that N294S and H274Y, two popular drug-resistant mutations in different variants of NA, still cause significant resistance to oseltamivir. However, the Y252H mutation does not impair the interactions between oseltamivir and A/H1N1 NA. An examination of individual energy components shows that the loss of polar interactions is the key source for the resistance of the studied mutations to oseltamivir. Moreover, free energy decomposition analysis and structural analysis reveal that the N294S or H274Y mutation triggers the large-scale conformational changes of the binding pocket and then impairs the affinity of oseltamivir. We expect that our results will be useful for the rational design of NA inhibitors with high potency against drug-resistant A/H1N1 mutants.

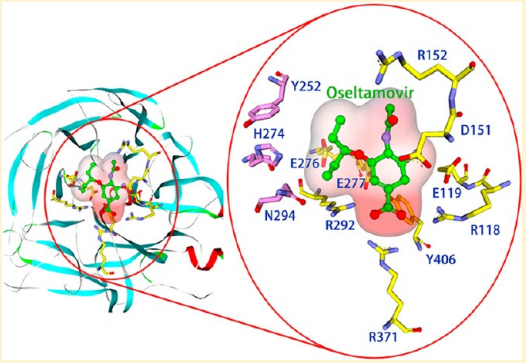

INTRODUCTION

Influenza virus is highly contagious and can lead to severe respiratory infection and even death. Every decade or so, a dangerous new strain appears and poses a threat to public health. Since March 2009, there has been an outbreak of a new strain of the influenza A/H1N1 virus, more commonly known as swine influenza. The rapid spread of the A/H1N1 swine influenza has affected over 214 countries and caused over 18 449 fatalities.[1] This new subtype A/H1N1 is a recombined virus from human, swine, and avian influenza viruses with a high transmissible ability among human beings, and it is continually changing.[2]

The influenza virus can be classified by the serological reactivity of its surface glycoprotein antigens such as hemagglutinin (HA) and neuraminidase (NA).[3] So far, 16 subtypes of HA (H1−H16) and nine subtypes of NA (N1−N9) circulating in avian and mammalian hosts have been identified.[4] Of the nine avian NA subtypes, only N1 and N2 have been found in human viruses responsible for pandemics and recurrent annual epidemics.[5] NA cleaves the terminal linkage between sialic acid and the virus, resulting in a release of viral progeny and further spread of infection.[6] Due to the importance of NA in limiting the progression of influenza virus infection in the host, NA has become an attractive target for the structure-based design of antiviral drugs.[4,7−10]

To date, only four antiflu drugs have been approved by the Food and Drug Administration (FDA): amantadine (symmetrel) and rimantadine (flumadine),[11] which both target the M2 ion channel of the influenza A virus, and oseltamivir (tamiflu)[12] and zanamivir (relenza),[13] which both inhibit NA. Among these drugs, oseltamivir is recommended by the World Health Organization (WHO) and the Centers for Disease Control and Prevention (CDC) as the most effective antiviral agent for the treatment of infected patients and has shown effectiveness for 2009 influenza A/H1N1 virus.[14,15]

It is well-known that when antiflu drugs are widely used, the influenza virus evolves quickly. NA also faces a selection pressure, and possible mutants will occur.[6,16,17] Some NA mutants can cause resistance to the available drugs. For

Received: June 4, 2012
Published: September 22, 2012

example, the oseltamivir-resistant N294S and H274Y mutations in NA have been identified in the A/H3N2, A/H5N1, and A/H1N1 viruses.[18−22] The emergence of the oseltamivir-resistant NAs for A/H1N1 indicates that oseltamivir currently in use may not fully protect humans. Once the drug-resistant strains occur, they will probably lead to a large scale outbreak of novel pandemic influenza.[23] Thus, a new generation of anti-influenza drugs is needed. However, to develop improved antiviral reagents, we need to understand the molecular mechanisms of oseltamivir resistance in the A/H1N1 virus.

Molecular modeling approaches, such as molecular dynamics (MD) simulations and free energy calculations, have been employed to study the interactions between inhibitors and the catalytic core domain of neuraminidase[24−29] and identify the novel druggable loop domain in neuraminidase.[10,30−34] Moreover, in recent years, theoretical approaches have been widely used to elucidate the mechanisms of drug resistance for different drug targets, including NA.[14,32,35−43] Shu et al. analyzed in detail the dynamic behavior of the wild-type (WT) and H252Y mutated NA complexes with oseltamivir.[29] Woods et al.[44] used long-time-scale MD simulations to understand, at a molecular level, how the I223R/H275Y mutations in NA can lead to drug resistance. The results from these long-time-scale MD simulations suggest that the efficacy of oseltamivir is reduced significantly because of conformational changes that lead to the open form of the 150-loop. Karthick et al. highlighted the effect of point-mutation-induced oseltamivir resistance in H1N1 subtype neuraminidases by molecular docking and MD simulations.[45] Malaisree et al. studied the dynamic nature of three inhibitors, oseltamivir, zanamivir, and peramivir, in the active site of N1 neuraminidase using MD simulations and molecular mechanics/Poisson−Boltzmann surface area (MM/PBSA) binding free energy calculations, and the ordering of the predicted binding free energies for the studied inhibitors agrees with the ordering of experimental data.[24] Lawrenz et al. then employed independent-trajectory thermodynamic-integration (IT-TI) calculations to investigate the N1-peramivir binding determinants and quantify their thermodynamic role in the binding process, and their results suggested that the most reliable and predictive free energy calculations will likely rely on the use of explicit solvent simulations and MD force fields based also on a direct and general parametrization of solvation thermodynamics.[28] Liu and co-workers used MD simulations and the molecular mechanics/generalized Born surface area (MM/GBSA) approach to identify the residues in 2009 A/H1N1 with significant contribution to the binding of substrate and inhibitors, and the potential drug resistance sites for two inhibitors were identified by analyzing the difference of interaction profiles of substrate and inhibitors.[14]

The computational studies of A/H5N1 NA resistance to oseltamivir have also been extensively reported;[26,46−50] however, the theoretical studies of 2009 A/H1N1 NA resistance to oseltamivir are still quite limited.[14,51] In this study, we intended to characterize the interactions between oseltamivir and the WT NA and the H274Y, N294S, and Y252H mutants of NA from the A/H1N1 virus by using molecular modeling techniques. The H274Y and N294S mutations were regularly identified in N1 (in NA group 1) after the treatment of oseltamivir, and Y252H was found in the H5N1 viruses isolated from infected humans in Vietnam and Cambodia in 2004 and 2005.[22,23,52−56] To elucidate the molecular mechanisms of drug resistance, we tried to quantify the resistance in terms of changes in the binding free energy of protein−oseltamivir complexes. To achieve this goal, MD simulations and free energy calculations were employed to evaluate the binding of oseltamivir to the WT NA and the three variants of NA from the A/H1N1 virus. Moreover, free energy decomposition analysis was used to determine the inhibitor−protein interaction spectra, which can help to understand the detailed interaction profiles and characterize the contribution of each residue for the binding of oseltamivir. On the basis of the results, the molecular mechanisms of the drug resistant mutations in 2009 A/H1N1 NA were extensively discussed.

MATERIALS AND METHODS

Preparation of the Initial Structures. The amino acid sequence of the WT 2009 A/H1N1 NA was retrieved from the NCBI protein database (accession no. ACP44158.1),[57] but its crystal structure has not been determined yet. The sequence similarity search for A/H1N1 NA against other sequences with available structural information was performed using the Discovery Studio 2.5 molecular simulation package,[58] which shows that A/H1NA NA has very high sequence identity (92%) with A/H5N1 NA, and therefore, the crystal structure of A/H5N1 NA in complex with oseltamivir (PDB entry: 3cl0[22]) was used as the template to model the homology model of A/H1N1 NA in Discovery Studio 2.5. First, the sequence alignments (Figure S1 in the Supporting Materials) between A/H1N1 NA and A/H5N1 NA were performed using the *multiple sequence alignments protocol* in Discovery Studio. Then, the crystal structure of A/H5N1 NA in complex with oseltamivir was structurally aligned with the theoretical model of A/H1N1 NA, and oseltamivir and calcium ions were extracted from the crystal structure and merged into the homology model of A/H1N1 NA. The root-mean-square deviation (RMSD) between the homology model after minimization and the template is 0.22 Å. Next, the H274Y, N294S, or Y252H mutant of A/H1N1 NA in complex with oseltamivir was generated by mutating the corresponding amino acid in the WT A/H1N1 complex. The constructed models (WT and three mutants) were used as the initial structures for the following MD simulations (Figure 1).

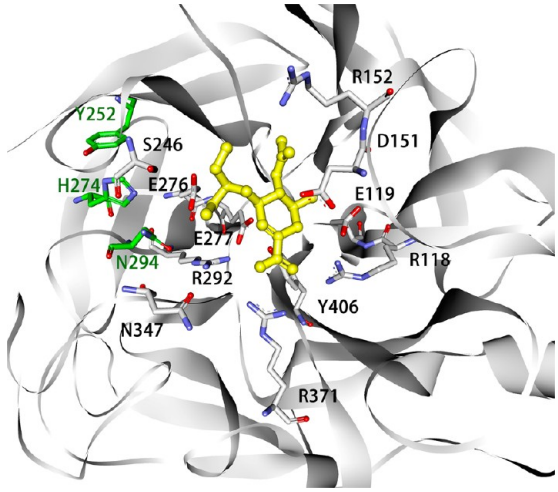

Figure 1. Modeled structure of WT A/H1N1 NA in complex with oseltamivir. Some key residues for ligand binding are labeled, and the carbon atoms of the three mutated residues studied in this work are colored in green.

MD Simulations. In our study, all hydrogen atoms of the proteins were added using the *tleap* program in AMBER11.[59] Eight disulfide bonds in each protein were properly enforced using the CYX notation in AMBER11.[59] The protonated states for the histidine residues were determined at pH 6.5 with the PDB2PQR[60] Web server using PROPKA[61] and were manually verified. The AMBER03 force field was employed for the proteins[62] and the general AMBER force field (*gaff*) for oseltamivir.[63] Oseltamivir was optimized by quantum calculations at the HF/6-31G* level,[64] and then the atomic partial charges were obtained by fitting the electrostatic potentials using the RESP fitting technique in AMBER11.[65] The generations of the partial charges and the force field parameters for oseltamivir were accomplished using the *antechamber* program in AMBER11.[59] The atom types and partial charges for oseltamivir are listed in Table S1 in the Supporting Materials. To neutralize the systems, two counterions of Cl^- were placed in the grids with the strongest negative Columbic potentials around the protein. The parameters for Cl^- were based on the values reported by Åqvist, adjusted for Amber's nonbonded atom pair combining rules to give the same ion−water potentials as in the original study.[66] Each system was solvated using a rectangular box of TIP3P water molecules,[67] and the water box was extended 10 Å from solute atoms in all three dimensions. Then, the initial coordinates and topology files were generated using the *tleap* program in AMBER11.[59]

Subsequently, to remove bad contacts, the system was minimized with the following protocol. During the first phase of the minimization, only the hydrogen atoms were minimized for 1000 steps, and the other atoms were fixed; then, the hydrogen atoms, the water molecules, and the ions were relaxed for 1000 steps. Next, the protein backbone was fixed, and all of the other atoms were minimized for 1000 steps. Finally, the whole system was relaxed using 5000 steps of minimization without any constraint.

After optimization, the system was gradually heated in the NVT ensemble from 0 to 300 K over 50 ps. Then, 50 ps MD simulations were preformed in the NPT ensemble, with the target temperature at 300 K and the target pressure at 1.0 atm.[68] Finally, we ran 70 ns MD simulations with the target temperature at 300 K and the target pressure at 1.0 atm. Electrostatics was handled using the particle mesh Ewald (PME) algorithm with an 8.0 Å direct-space nonbonded cutoff.[69] All bonds involving hydrogen atoms were constrained using the SHAKE algorithm,[70] permitting a time step of 2.0 fs. Coordinate trajectories were saved every 10 ps during the whole MD runs. The MM optimization and MD simulations were accomplished using the *sander* program in AMBER11.[59]

MM/PBSA Binding Free Energy Calculation. To better understand the molecular mechanisms of drug resistance, we intended to quantify the resistance in terms of changes in the binding free energy of protein−ligand complexes. Compared with more theoretically rigorous approaches, such as free energy perturbation (FEP)[71−74] and thermodynamic integration (TI) methods,[75,76] the MM/PBSA and MM/GBSA approaches are more computationally efficient.[77−82] The speed gained by MM/PBSA or MM/GBAS methods is achieved at the cost of some accuracy by making more crude assumptions on the binding compared with FEP and TI, but the MM/GBSA or MM/PBSA approaches can provide some information on relative binding affinities. So the MM/GBSA or MM/PBSA methods that are not rigorous can also be efficient. Similar to MM/PBSA and MM/GBSA, the linear interaction energy (LIE) method restricts the simulations to the two end points of ligand binding. However, the LIE method is an empirical method and needs the experimental binding free energy of several inhibitors or several mutations to obtain the involved parameters of the equation.[83−86] MM/PBSA or MM/GBSA is advantageous in that it can be used for many types of intermolecular complexes and that it is "universal" and does not require fitting of additional parameters.[78−80,82]

MM/PBSA has been successfully applied to the NA systems.[27,31,32,47,87] The binding energy ($\Delta G_{binding}$) in our study was estimated on the basis of the obtained stable MD trajectory for each protein−oseltamivir complex using the MM/PBSA technique implemented in AMBER11.[59] The snapshots of complex, receptor, and ligand were extracted from a single trajectory of the complex, and the binding free energy ($\Delta G_{binding}$) between a ligand and a receptor is calculated with the following equation:

$$\Delta G_{binding} = \Delta H - T\Delta S \approx \Delta E_{MM} + \Delta G_{sol} - T\Delta S$$
$$\Delta E_{MM} = \Delta E_{int\ ernal} + \Delta E_{ele} + \Delta E_{vdw}$$
$$\Delta G_{sol} = \Delta G_{PB} + \Delta G_{SA} \quad (1)$$

where ΔE_{MM}, ΔG_{sol}, and $-T\Delta S$ are the changes of the gas phase MM energy, the desolvation free energy, and the conformational entropy upon binding, respectively. ΔE_{MM} includes $\Delta E_{internal}$ (bond, angle, and dihedral energies), ΔE_{ele} (electrostatic), and ΔE_{vdw} (van der Waals) energies. ΔG_{sol} is the sum of electrostatic solvation energy (polar contribution), ΔG_{PB}, and the nonelectrostatic solvation component (nonpolar contribution), ΔG_{SA}. A common strategy to reduce noise and cancel errors in simulations is to run MD simulations on the complex only. Snapshots taken from this single trajectory of MD simulation are used to calculate each free energy component in the above equations. In such a single trajectory approach, $\Delta E_{internal}$ is canceled between ligand, receptor, and complex, which can significantly reduce the noise in most cases.[36,79,82]

The polar contribution by solving the PB equation was calculated using the *pbsa* program in Amber11.[88] We used 80 for the exterior dielectric constant, and 1 for the solute dielectric constant. The nonpolar part of desolvation was estimated by solvent accessible surface area (SASA) using the LCPO method with a water probe radius of 1.4 Å: ΔG_{SA} = 0.0378 × ΔSASA. Here, the conformational entropy change $-T\Delta S$ was not considered because of its extensive computational cost and low prediction accuracy.[89−91] For the calculations of ΔE_{MM}, ΔG_{GB}, and ΔG_{SA}, 500 snapshots evenly extracted from the single MD trajectory of each complex from 30 to 70 ns were used. Within the MM/PBSA approach, the free energy is additive, containing contributions from different types of interactions. Such a decomposition is useful for understanding the nature of complex systems and is also possible in the more rigorous free energy perturbation approach.[92,93]

MM/GBSA Binding Free Energy Decomposition. To obtain the contribution of each residue to binding energy, MM/GBSA was used to decompose the interaction energies to each residue involved in the interaction by considering molecular mechanics and solvation energies without consideration of the contribution of entropies.[94−98] The energy contribution of each residue was decomposed into four terms: van der Waals contribution (ΔG_{vdw}), electrostatic contribution

(ΔG_{ele}), and polar (ΔG_{GB}) and nonpolar (ΔG_{SA}) contribution of desolvation.

$$\Delta G_{residue-inhibitor} = \Delta G_{vdw} + \Delta G_{ele} + \Delta G_{solvation} = \Delta G_{vdw} + \Delta G_{ele} + \Delta G_{GB} + \Delta G_{SA} \quad (4)$$

where ΔG_{vdw} and ΔG_{ele} are nonbonded van der Waals and electrostatic interactions between the inhibitor and each residue, respectively, and can be computed using the *sander* program in AMBER11. The electrostatic desolvation energy (ΔG_{GB}) was estimated by using the GB model based on the parameters developed by Onufriev et al. (igb=2 in AMBER11).[99] The nonpolar contribution of desolvation (ΔG_{SA}) was determined from the solvent accessible surface area (SASA) using the ICOSA technique.[95]

RESULTS AND DISCUSSION

1. Structural Flexibility and Stability. To check whether the equilibrated MD trajectory was stable, the root-mean-square deviations (RMSDs) for the backbone atoms of each protein during the production phase relative to the initial coordinates were calculated for the four studied systems. Moreover, the RMSDs of the active site residues are also illustrated in Figure S2. The RMSD plots (Figures 2 and S2)

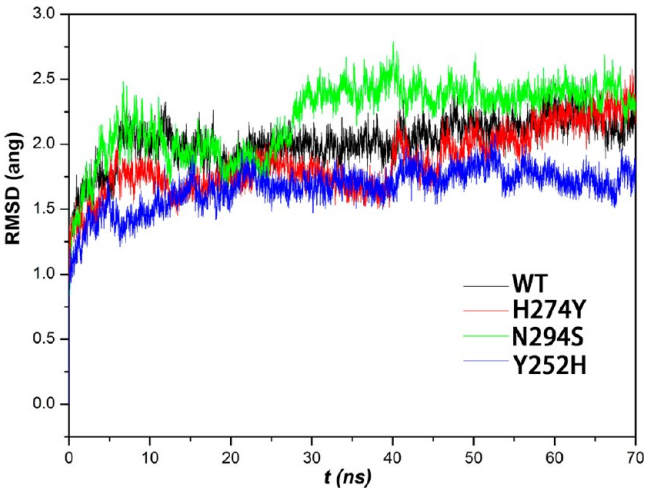

Figure 2. RMSD of the backbone atoms of NA with respect to the first snapshot as a function of time (black, red, green, and blue lines represent WT, H274Y, N294S, and Y252H, respectively).

indicate that all of the four studied systems had reached equilibrium after about ~30 ns. The averaged RMSD values from 30 to 70 ns MD simulations are 2.11 Å, 1.98 Å, 2.39 Å, and 1.74 Å for WT, H274Y, N294S, and Y252H complexes, respectively. It must be noted that a stable RMSD does not always indicate that the binding free energies are stable. In particular, for an approach such as MM/PBSA that uses the converged energies to compute binding affinities and rank them, the stability of the energy is much more significant than that of the trajectory. The fluctuations of the total nonpolar ($\Delta E_{vdw} + \Delta G_{SA}$) interactions and total polar ($\Delta E_{ele} + \Delta G_{PB}$) interactions between oseltamivir and the H274Y NA are illustrated in Figure 3, and those for the other systems are provided in Figure S3 as Supporting Information. The electrostatic interactions (ΔE_{ele}) are anticorrelated to the opposing electrostatic desolvation energies (ΔG_{PB}), and

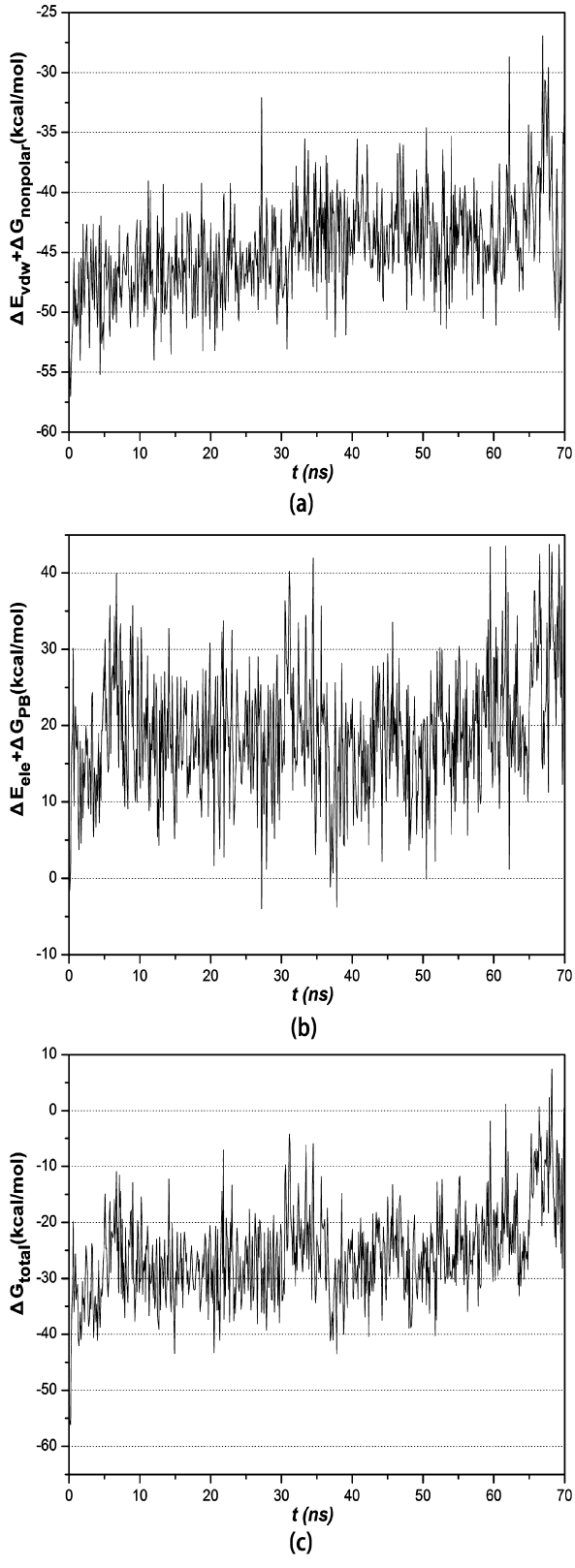

Figure 3. Fluctuations of the (a) total nonpolar ($\Delta E_{vdw} + \Delta G_{SA}$), (b) total polar ($\Delta E_{ele} + \Delta G_{PB}$), and (c) total binding energy (ΔG_{total}) interactions between oseltamivir and the H274Y NA.

therefore, the sum of ΔE_{ele} and ΔG_{PB} is more stable than the ΔE_{ele} or ΔG_{PB} term. It can be found in Figure 3 that the energy terms are relatively stable, but obvious fluctuations still can be

Table 1. The Binding Free Energy Components Predicted by MM/PBSA (kcal/mol)

	polar contributions		nonpolar contributions			
system[a]	ΔE_{ele}[b]	ΔG_{PB}	ΔE_{vdw}	ΔG_{SA}	$\Delta G_{binding}$ (pred)	IC_{50} (nM)[105]
WT	−119.54 ± 3.67	129.00 ± 4.45	−23.00 ± 0.46	−22.35 ± 0.12	−35.88 ± 1.13	0.46 ± 0.01
H274Y	−138.65 ± 9.49	158.34 ± 7.18	−21.65 ± 0.10	−21.38 ± 0.44	−23.34 ± 2.64	451.9 ± 26.0
N294S	−147.44 ± 1.55	167.85 ± 2.78	−23.55 ± 1.08	−22.07 ± 0.61	−25.21 ± 2.91	95.8 ± 5.4
Y252H	−141.06 ± 6.98	153.73 ± 3.67	−24.67 ± 1.12	−23.39 ± 0.08	−35.39 ± 2.11	0.032[c]

[a]All mutations are presented in A/H5N1 NA numbering. [b]The standard deviations for all energy terms were calculated on the basis of two blocks (block1: 31−50 ns; block2: 51−70 ns). [c]Experimental K_i value for A/H5N1 NA[22]

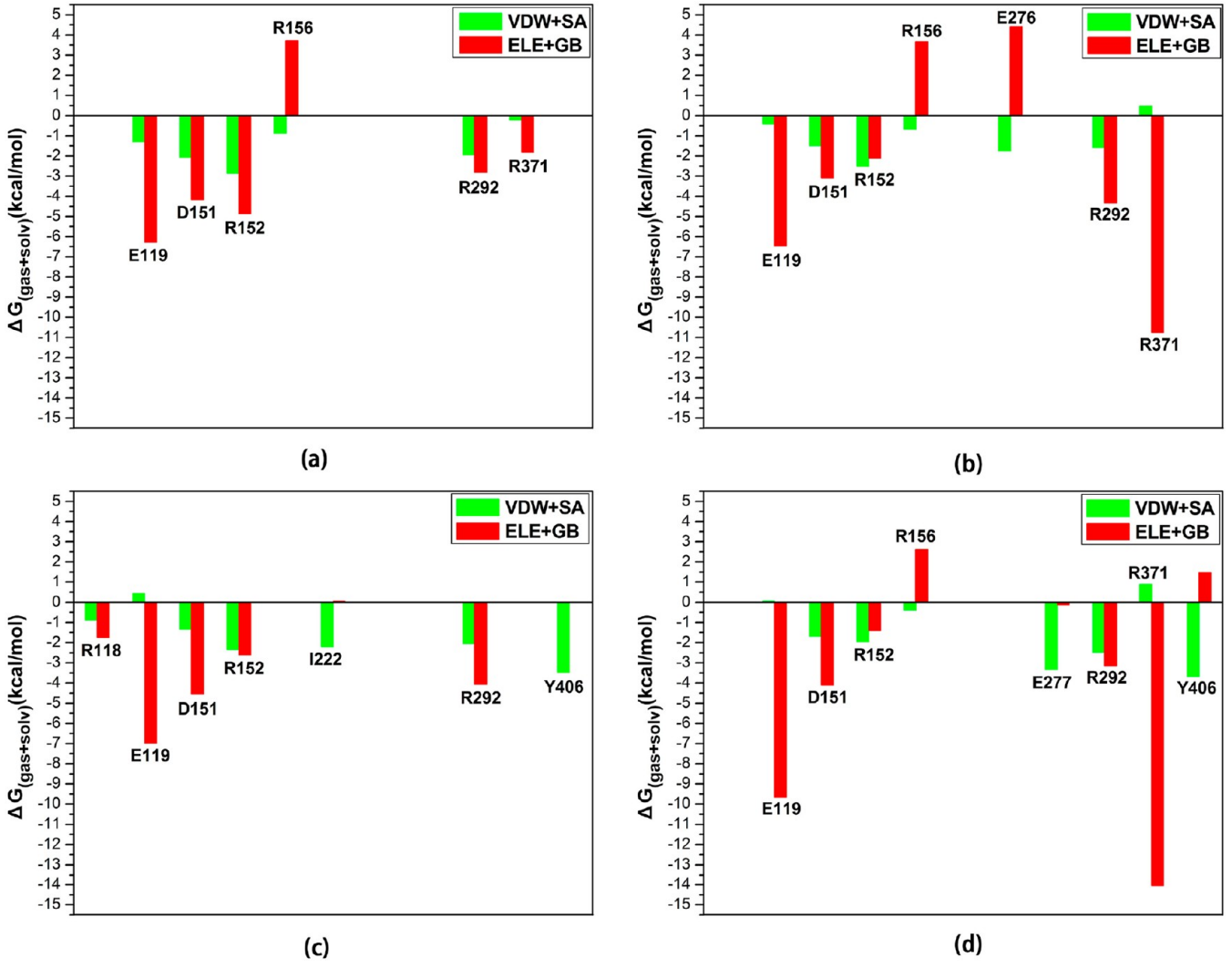

Figure 4. Contributions of the important residues to the total binding free energies (the residues with $|\Delta G| \geq 2.0$ kcal/mol are labeled) for the (a) WT, (b) H274Y, (c) N294S, and (d) Y252H complexes.

observed. Therefore, we believe that relatively long MD simulations are necessary to achieve stable predictions.

2. The Predicted Binding Free Energies. The binding free energy components of the studied systems predicted by the MM/PBSA method are listed in Table 1. It can be observed that the electrostatic and van der Waals terms are favorable for the oseltamivir binding, whereas the polar contribution of desolvation opposes binding strongly, and the nonpolar desolvation term also contributes favorably. By comparing the total polar (ΔE_{ele} + ΔG_{PB}) contributions with the total nonpolar (ΔE_{vdw} + ΔG_{SA}) contributions, we observe that the primary contributor to $\Delta G_{binding}$ is the nonpolar interaction, particularly the ΔE_{vdw} term.

The binding affinities of the mutated H274Y and N294S complexes are −12.54 kcal/mol and −10.67 kcal/mol weaker than that of the WT complex, while the binding affinity of the Y252H mutant is almost the same as that of the WT complex, indicating that the H274Y and N294S mutations impair the binding of oseltamivir and lead to drug resistance, whereas the Y252H mutant shows nonresistance. It is encouraging to note that the order of the experimental affinities of all the complexes is well consistent with that of our calculated binding free energies.

dx.doi.org/10.1021/ci300375k | J. Chem. Inf. Model. 2012, 52, 2715−2729

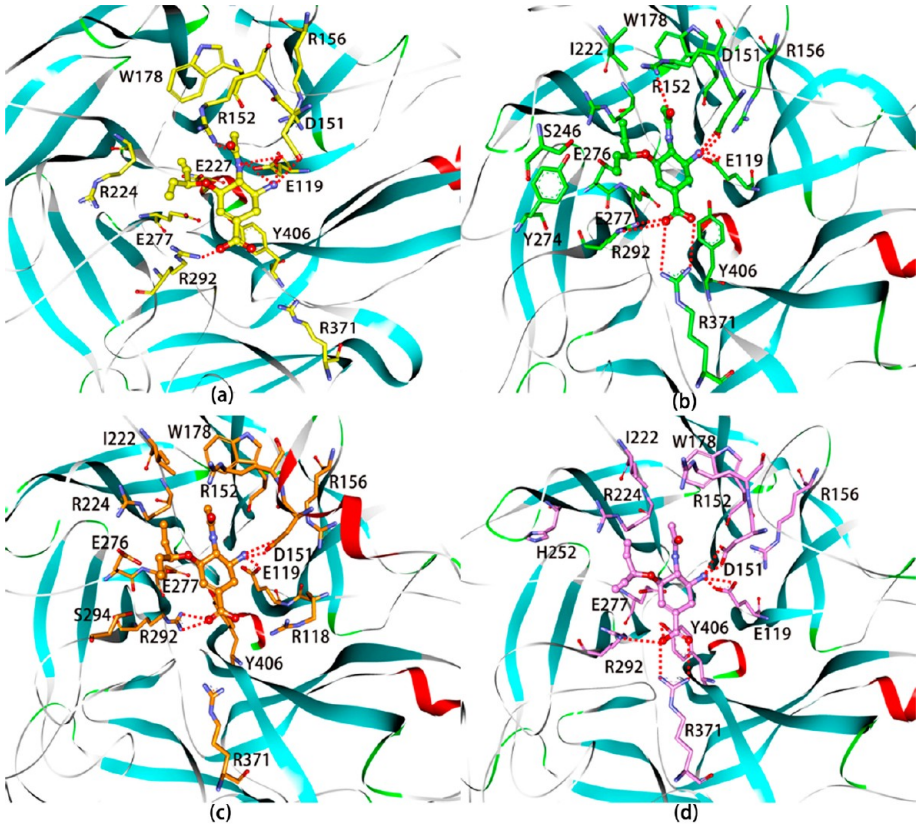

Figure 5. Geometries of the important residues that form strong interactions with oseltamivir for the (a) WT, (b) H274Y, (c) N294S, and (d) Y252H complexes. The averaged structures extracted from the MD trajectories were used. Oseltamivir is shown as ball-and-stick, and the hydrogen bonds are highlighted by the dashed lines.

The free energy components of the WT complex and each mutated complex were compared to elucidate the mechanism to drive the drug resistance. According to our analysis, we can make the following conclusion: the differences of the nonpolar desolvation energies among the four systems are not significant and the difference of the binding free energies is primarily associated with the loss of the polar interactions. For example, the polar term for the H274Y complex decreases about 10.23 kcal/mol compared with that for the WT complex, which should be essential for the resistance of H274Y to oseltamivir. Then, we compared the correlations between the predicted binding free energies and individual energy component. We found that the polar contributions ($\Delta E_{ele} + \Delta G_{PB}$) have much higher correlation ($r^2 = 0.93$) with the binding free energies than the nonpolar contributions ($r^2 = 0.50$), suggesting that the polar contributions determine the difference of the binding affinities of the studied systems. In Kar and Knecht's work,[31] they suggested that the drug resistance of Y252H, H274Y, and R292K of the N8 neuraminidase was correlated with the unfavorable shifts in the intermolecular electrostatic interactions. In Wang and Zheng's work,[47] the authors proposed that the differences between the binding free energy of oseltamivir in the WT complex of H5N1 NA and that in the H274Y or N294S complex of H5N1 NA are largely controlled by the electrostatic component, which are also consistent with our calculation results.

3. Essential Residues for Oseltamivir Binding. In order to get a deeper insight into the protein−inhibitor interaction patterns, the total binding free energy was decomposed into inhibitor−residue pairs based on MM/GBSA. As shown in Figures S4−S7, the inhibitor−residue interaction spectra of the studied complexes are quite similar. Overall, the favorable residues include R118, E119, D151, R152, W178, S179, I222, R224, E227, S246, E276, E277, R292, N294, R371, and Y406, and most of these residues are located in the binding site of NA and can form direct contacts with oseltamivir that were also proven experimentally by other groups.[45,100] Generally, the binding residues of NA are composed of four zones: (1) R118, R292, R371, and Y406; (2) E119 and D151; (3) R152 and W178; and (4) R224 and E276, which interact with the $-COO^-$, $-NH3^+$, −NHAc, and $-OCHEt_2$ groups of oseltamivir, respectively.

Figure 4 shows the decomposition of $\Delta G_{binding}$ into the contributions of the polar ($\Delta E_{ele} + \Delta G_{PB}$) and nonpolar ($\Delta E_{vdw} + \Delta G_{SA}$) interactions for the residues with $|\Delta G_{binding}| \geq 2.00$ kcal/mol. According to Figure 4, we can observe that the interactions between oseltamivir and proteins are primarily contributed by about 11 residues in total. Among these important residues, residues E119, D151, R152, and R292 can be found in all systems. The main favorable binding forces of R156 in Figure 4a, b, and d are the sum of the van der Waals (ΔE_{vdw}) and nonpolar desolvation energy (ΔG_{SA}), while the polar contributions ($\Delta E_{ele} + \Delta G_{PB}$) are more unfavorable. Similar to R146, the polar contributions of E276 in Figure 4b and those of Y406 in Figure 4d are unfavorable, but the unfavorable nonpolar contributions of Y406 in Figure 4d can be effectively compensated by the favorable polar contributions. The main driving force of Y406 in Figure 4c is the nonpolar contributions, and similar results can be obtained for I222 and E277 in Figure 4c and d. The nonpolar contributions of R371

in Figure 4b and d and those of E119 in Figure 4c and d are unfavorable for binding. For the other residues in Figure 4, both of the polar and nonpolar contributions are favorable for binding, but the polar contributions are much more favorable.

Figure 5 depicts the geometry of oseltamivir in the binding site with the relevant residues for the WT and different mutants. The detailed analysis of the energy decomposition results is present in the next section.

4. The Mechanism of Drug Resistance. In order to make a full investigation of the influence of the H274Y, N294S, or Y252H mutation on the interaction of oseltamivir, the inhibitor−residue spectra for the WT/oseltamivir complex and each mutated complex were compared systematically. The inhibitor−protein interaction spectra are illustrated in Figures S4−S7, and the numerical data are summarized in Table S2 in the Supporting Information.

The H274Y Mutation. For the H274Y complex, the predicted binding free energy of oseltamivir (Table 1) is ~12.54 kcal/mol more unfavorable than that for the WT complex. Our simulated binding structures (Figure 5a and b) show that the negatively charged carboxylate of oseltamivir interacts strongly with R371 and R292 in the H274Y complex, while it only forms a hydrogen bond with R292 in the WT complex, which is consistent with the data shown in Figures S4 and S5 and Table S2. The ammonium group of oseltamivir forms two stable hydrogen bonds not only with the negatively charged carboxyl group of E119 but also with the carboxyl group of D151 in both of the WT and the H274Y complexes, which is consistent with Shu's study that the ammonium group of oseltamivir in the wild-type complex is stabilized by the hydrogen bonding interactions with the two negatively charged residues Glu119 and Asp151. In the work reported by Masukawa et al.,[27] the hydrogen bonds with Asp151 were also found in different neuraminidase complexes. The acetamide group of oseltamivir forms three hydrogen bonds with R152 and E119 in the WT complex, while it only forms a hydrogen bond with R152 in the H274Y complex. The analysis based on the simulated structures is consistent with the inhibitor−protein interaction spectra.

Figures 6−8 show the subtraction between the inhibitor−residue interactions of the WT/oseltamivir complex and that of a mutated complex. In total, there are six residues with large differences (Figure 6a). Among these six residues, three (D151, R152, and E276) in the WT complex have stronger interactions with oseltamivir than those in the H274Y complex, and the others (E277, R292, and R371) in the H274Y complex form stronger interactions with oseltamivir than those in the WT complex (the data are summarized in Table S2, and the spatial distribution of these six residues is shown in Figure 9a). It is interesting to find that the mutated residue itself does not have a significant effect on the change of ligand binding.

As shown in Table 1, the van der Waals interaction between oseltamivir and the H274Y mutant (−21.65 kcal/mol) is weaker than that between oseltamivir and the WT NA (−23.00 kcal/mol). When comparing the difference between the inhibitor−residue nonpolar interaction spectra of the WT and H274Y complexes (Figure 6b), we can find that there are 10 residues with an absolute value of the difference larger than 0.50 kcal/mol, in which three (R224, S246, and E276) are related to the decrease of oseltamivir binding with the WT H1N1, while the other seven (E119, D151, S179, *I*222, E227, E277, and R371) are responsible for the decrease of oseltamivir binding with the H274Y H1N1 (the data are summarized in

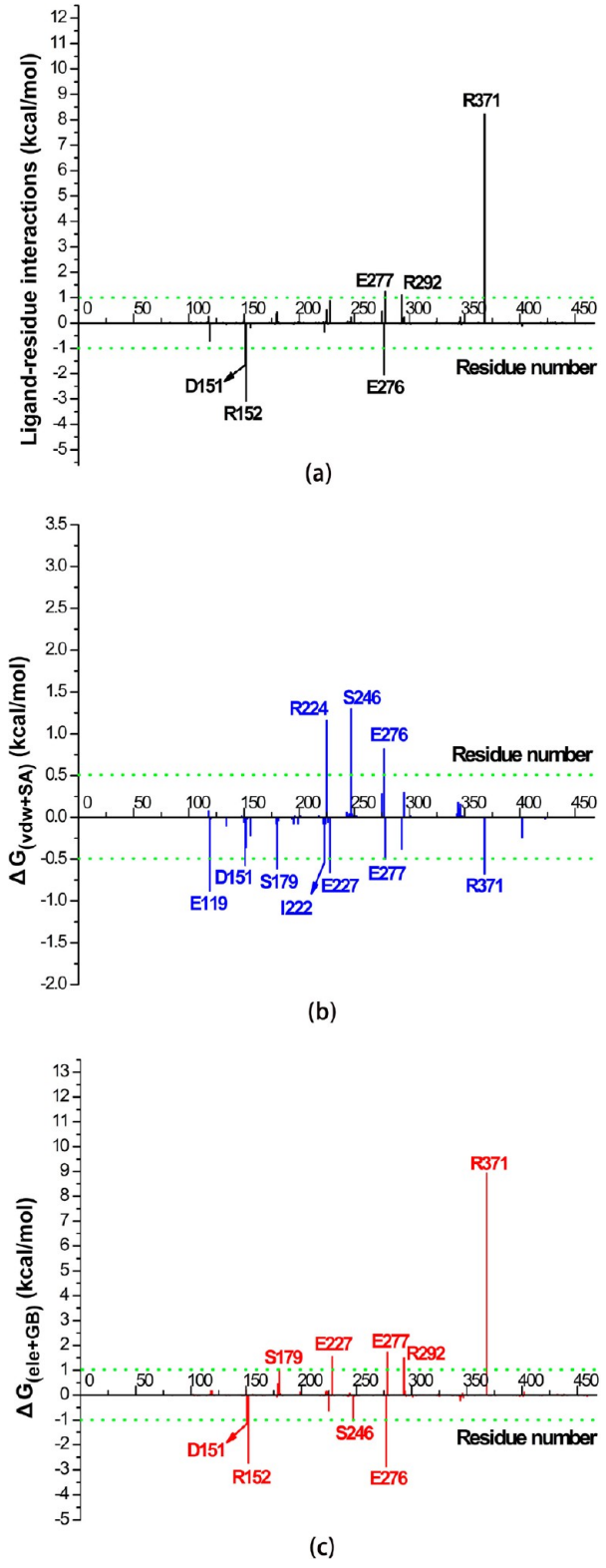

Figure 6. The distribution of the difference between the WT complex and that of the H274Y complex: (a, b, and c) The inhibitor−residue interactions, the inhibitor−residue nonpolar (ΔG_{vdw} + ΔG_{SA}) interactions, and inhibitor−residue polar (ΔG_{ele} + ΔG_{GB}) interactions, respectively. The residues with an absolute difference larger than 1 kcal/mol for the inhibitor−residue interactions and the polar (ΔG_{ele} + ΔG_{GB}) interactions are labeled by two cutoff lines, and the residues with an absolute difference larger than 0.5 kcal/mol for the inhibitor−residue nonpolar (ΔG_{vdw} + ΔG_{SA}) interactions are labeled by two cutoff lines.

dx.doi.org/10.1021/ci300375k | J. Chem. Inf. Model. 2012, 52, 2715−2729

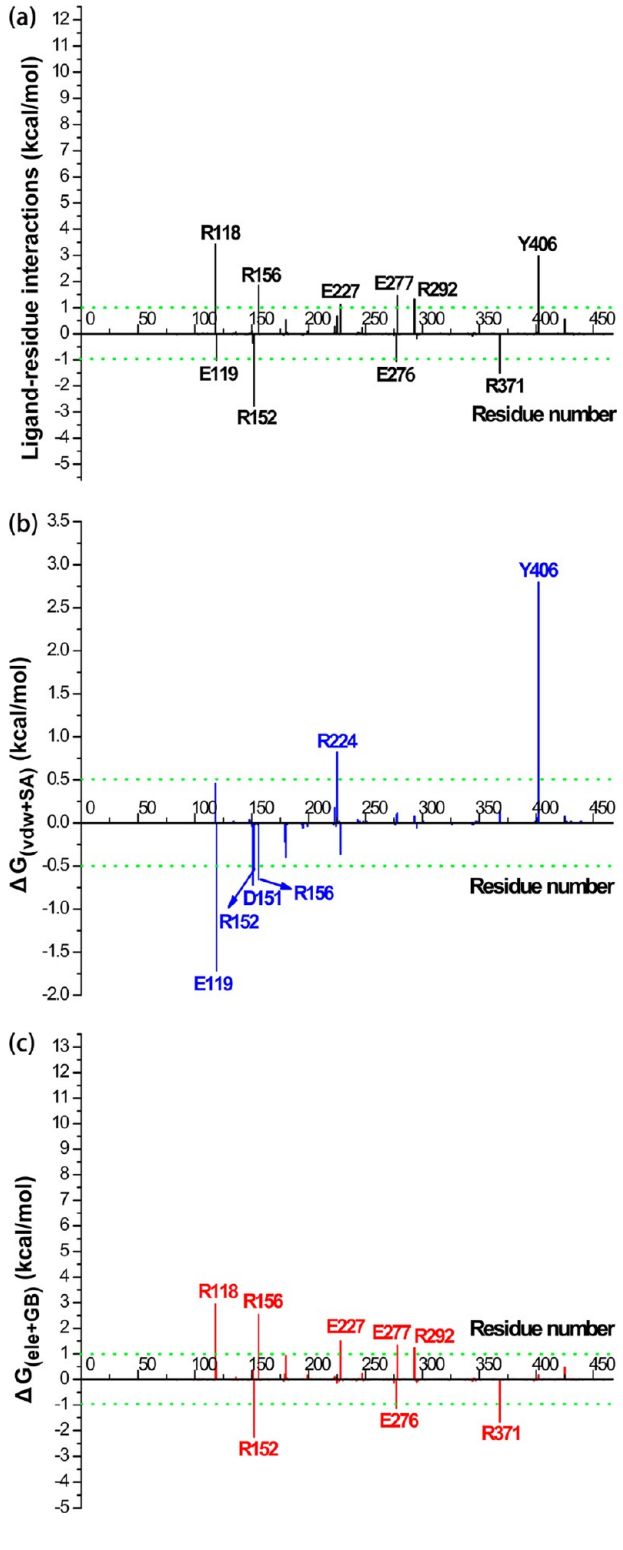

Figure 7. The distribution of the difference between the WT complex and that of the N294S complex: (a, b, and c) The inhibitor−residue interactions, the inhibitor−residue nonpolar (ΔG_{vdw} + ΔG_{SA}) interactions, and inhibitor−residue polar (ΔG_{ele} + ΔG_{GB}) interactions, respectively. The residues with an absolute difference larger than 1 kcal/mol for the inhibitor−residue interactions and the polar (ΔG_{ele} + ΔG_{GB}) interactions are labeled by two cutoff lines, and the residues with an absolute difference larger than 0.5 kcal/mol for the inhibitor−residue nonpolar (ΔG_{vdw} + ΔG_{SA}) interactions are labeled by two cutoff lines.

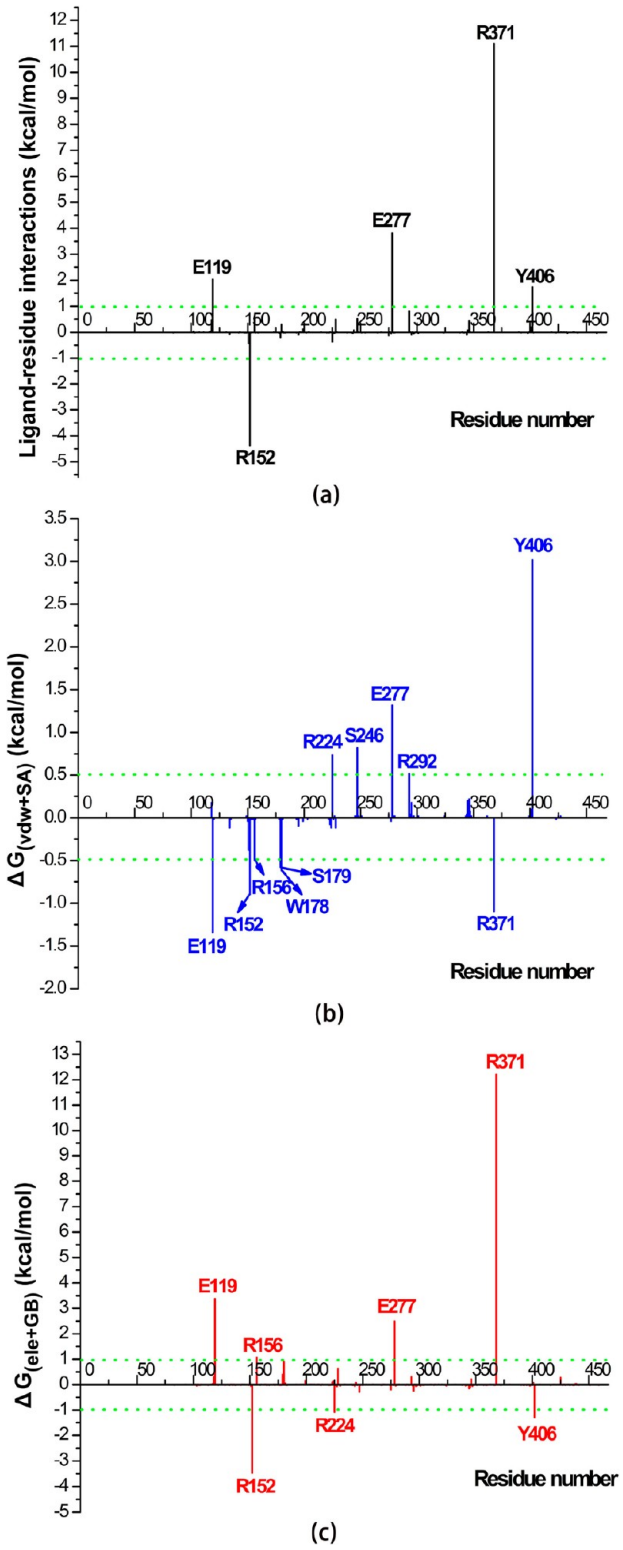

Figure 8. The distribution of the difference between the WT complex and that of the Y252H complex: (a, b, and c) The inhibitor−residue interactions, the inhibitor−residue nonpolar (ΔG_{vdw} + ΔG_{SA}) interactions, and inhibitor−residue polar (ΔG_{ele} + ΔG_{GB}) interactions, respectively. The residues with the absolute difference larger than 1 kcal/mol for the inhibitor−residue interactions and the polar (ΔG_{ele} + ΔG_{GB}) interactions are labeled by two cutoff lines, and the residues with the absolute difference larger than 0.5 kcal/mol for the inhibitor−residue nonpolar (ΔG_{vdw} + ΔG_{SA}) interactions are labeled by two cutoff lines.

dx.doi.org/10.1021/ci300375k | J. Chem. Inf. Model. 2012, 52, 2715−2729

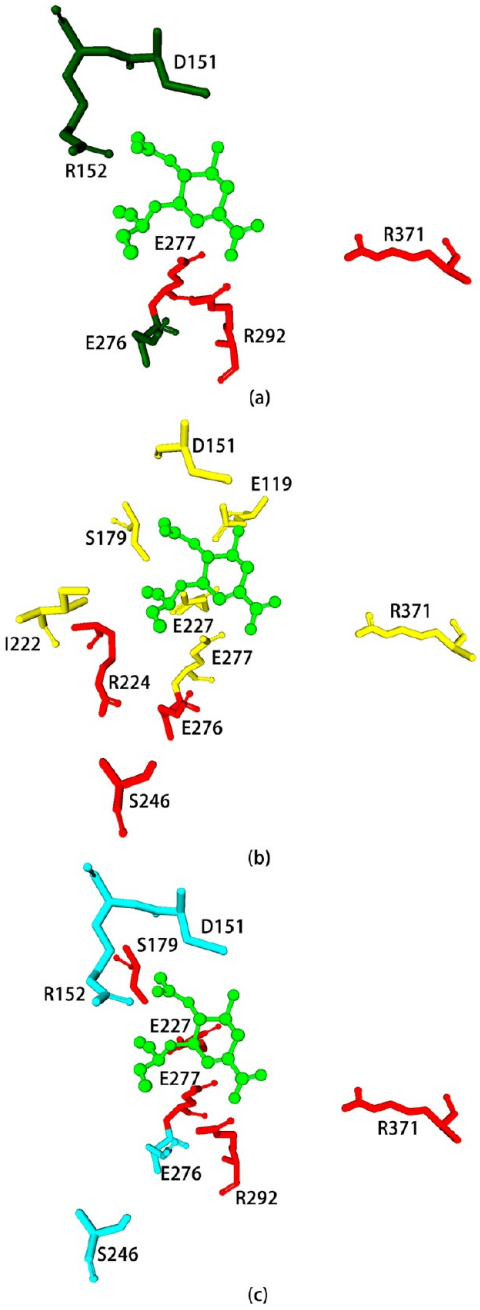

Figure 9. (a) Geometries of the six residues that contribute most to the difference between the inhibitor−residue interactions of the WT complex and those of the H274Y complex. (b) Geometries of the 10 residues that contribute most to the difference between the nonpolar (ΔG_{vdw} + ΔG_{SA}) inhibitor−residue interactions of the WT complex and those of the H274Y complex. (c) Geometries of the nine residues that contribute most to the difference between the total polar (ΔG_{ele} + ΔG_{GB}) inhibitor−residue interactions of the WT complex and those of the H274Y complex. The residues with stronger interactions with the H274Y complex are colored in red, and those with stronger interactions with the WT complex in atrovirens are colored yellow or blue. The structure of oseltamivir is shown as green ball-and-stick.

Table S2, and the spatial distribution of these 10 residues is shown in Figure 9b).

The comparison of the total polar interaction between the WT complex and the H274Y complex (Figure 6c) shows that there are nine important residues with an absolute value of the difference larger than 1 kcal/mol, and the spatial distribution of these nine residues is shown in Figure 9c. It is obvious that six important residues in Figure 9a can also be found in Figure 9c, suggesting that the H274Y mutation has much more effect on the polar interactions between oseltamivir and the H274Y mutant than on the nonpolar interactions between oseltamivir and the H274Y mutant. Among those six residues highlighted in Figure 9a, E277, R292, and R371 form stronger polar interactions in the H274Y complex than those in the WT complex, while D151, R152, and E276 form stronger polar interactions in the WT complex than those in the H274Y complex.

The mechanism of drug resistance of the H274Y mutation has been proposed in prior studies based on the crystal structures of H5N1 NA or influenza N1 neuraminidases in complex with oseltamivir[25,31,47,101−103] and experimental studies.[22] The hydrophobic R group of oseltamivir binds into a hydrophobic pocket formed by residues R224 and E276 that lie next to H274Y.[103] It has been suggested that the H274Y mutation reduces the size of the hydrophobic pocket and then leads to high resistance to oseltamivir.[25] It is believed that the resistance of H274Y might be the consequence of the conformational change of E276. The substitution by the bulkier tyrosine at position 274 pushes the side chain of E276 further into the binding site, and the conformational change of the side chain of E276 makes a consequent effect upon the shape and size of the hydrophobic pocket that normally accommodates the pentyloxy substituent of oseltamivir. Kar and Knecht[31] suggested that the binding pockets of the mutated N8 neuraminidases were slightly rigid or a nonflexible pocket compared to the binding pocket of the wild-type protein. These behaviors enable the wild structure to exhibit a stronger binding with oseltamivir than the mutated structure. According to Wang and Zheng's work,[47] the change of the desolvation energy caused by the reorientation of E276 is probably the primary contributor to the drug resistance caused by the H274Y mutation in H5N1 NA. In terms of drug resistance, our calculation results also support the mechanism of drug resistance described above. As shown in Figures 5b and 10a, the larger residue tyrosine in the H274Y complex obviously pushes the carboxyl groups of E276 in the WT complex toward the binding site and disturbs the hydrophobic pocket for accommodating the bulky −OCHEt$_2$ moiety of oseltamivir. At the mean time, the conformation of E277 is affected by the reorientation of E276, and the energy decomposition analysis shows that the polar contribution (0.10 kcal/mol) of E277 in the H274Y complex becomes more favorable compared with that (2.38 kcal/mol) in the WT complex. Moreover, as shown in Figure S6a, the conformations of oseltamivir and many adjacent residues, such as D151, R152, R292, and R371 in the H274Y complex, are obviously different from those in the WT complex (Figure 10 a). In summary, the replacement of H274 by a more bulky residue Tyr pushes E276 toward the −OCHEt$_2$ group, triggers an obvious structural change of the binding site, and then impairs the interactions between oseltamivir and NA.

The N294S Mutation. For the N294S complex, the predicted binding free energy of oseltamivir (Table 1) is ∼10.67 kcal/mol more unfavorable than that for the WT complex. The energy decomposition analysis shows that four residues are involved in the loss of the binding of oseltamivir caused by the N294S mutation, and they are E119, R152, E277, and R371 (Figures 7a and 11a). The energy contribution shows that the van der Waals interaction between oseltamivir and the

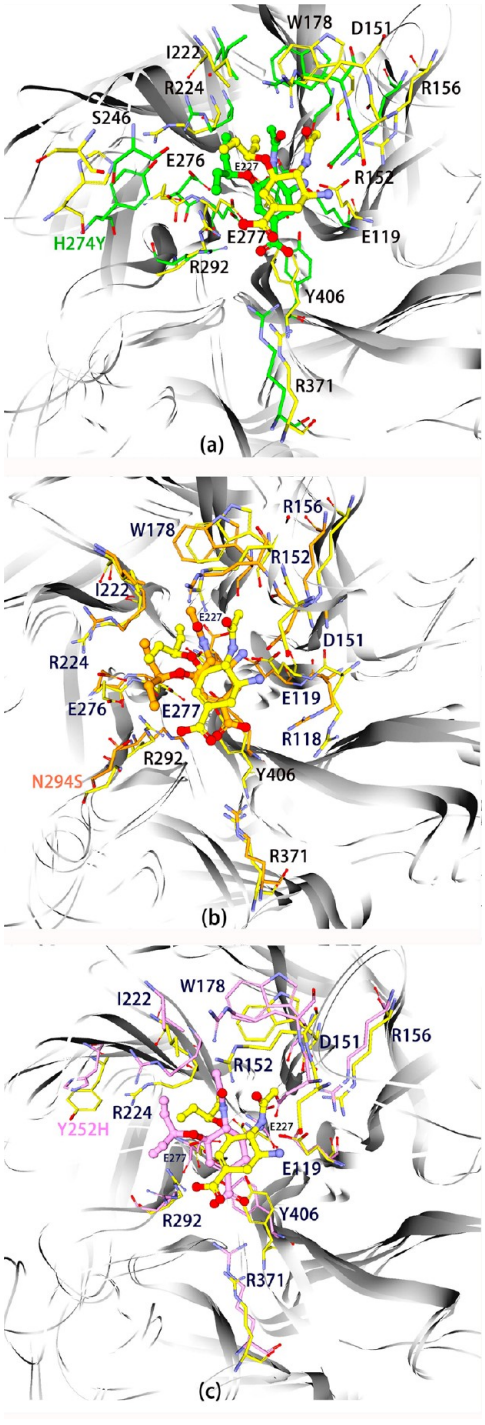

Figure 10. Superposition of the averaged MD structures of the WT/oseltamivir and (a) the H274Y/oseltamivir, (b) the N294S/oseltamivir, or (c) the Y252H/oseltamivir complex. The WT/oseltamivir, H274Y/oseltamivir, N294S/oseltamivir, and Y252H/oseltamivir complexes are shown in yellow, green, orange, and pink, respectively. Oseltamivir is shown as ball-and-stick, and the important residues are shown as sticks.

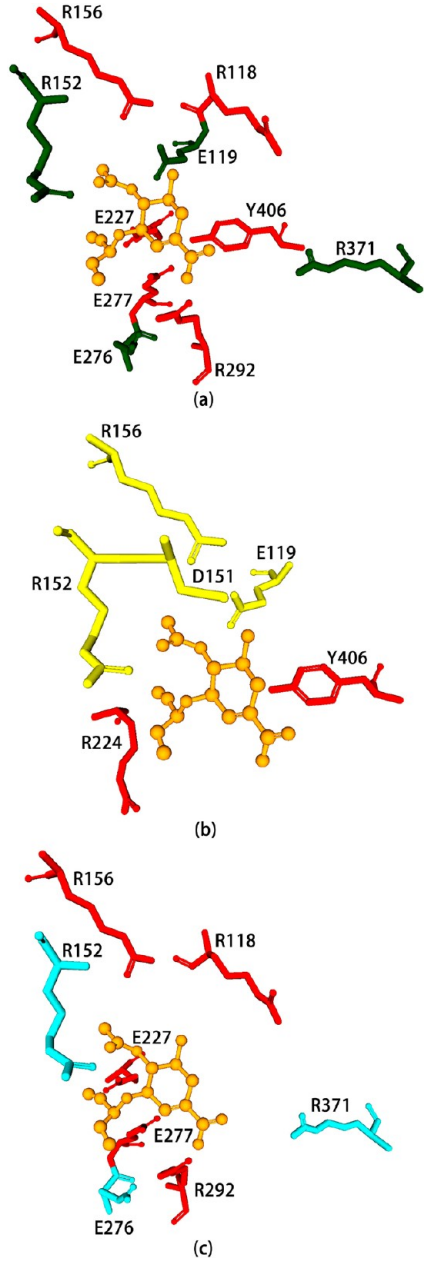

Figure 11. (a) Geometries of the 10 residues that contribute most to the difference between the inhibitor−residue interactions of the WT complex and those of the N294S complex. (b) Geometries of the six residues that contribute most to the difference between the nonpolar (ΔG_{vdw} + ΔG_{SA}) inhibitor−residue interactions of the WT complex and those of the N294S complex. (c) Geometries of the eight residues that contribute most to the difference between the total polar (ΔG_{ele} + ΔG_{GB}) inhibitor−residue interactions of the WT complex and those of the N294S complex. The residues with stronger interactions with the N294S complex are colored in red, and those with stronger interactions with the WT complex in atrovirens are colored yellow or blue. The structure of oseltamivir is shown as an orange ball-and-stick.

N294S mutant (−23.55 kcal/mol) is slightly stronger than that between oseltamivir and the WT NA (−23.00 kcal/mol). According to the data shown in Figure 7b, we can observe that there are six residues with the absolute values of the difference larger than 0.50 kcal/mol, among which, two (R224 and Y406) have stronger nonpolar interactions with oseltamivir in the N294S complex than those with oseltamivir in the WT complex, and four (E119, D151, R152, and R156) have stronger van der Waals interactions with oseltamivir in the WT complex than those with oseltamivir in the N294S complex. The spatial distribution of these six residues is shown in Figure 11b. The electrostatic interaction between oseltamivir and the

dx.doi.org/10.1021/ci300375k | J. Chem. Inf. Model. 2012, 52, 2715−2729

N294S mutant (−147.44 kcal/mol) is more favorable than that between oseltamivir and the WT NA (−119.54 kcal/mol). But when considering the polar contribution of desolvation together, the binding for the WT complex is about 10.95 kcal/mol more favorable than that for the N294S complex. The comparison of the total electrostatic interactions between the WT/oseltamivir and the N294S/oseltamivir complexes shows that there are eight important residues (R118, R152, R156, E227, E276, E277, R292, and R371) contributing most to the difference between the polar interactions of the WT complex and those of the N294S complex (Figures 7c and 11c).

The replacement of asparagine with serine makes the carboxyl group of oseltamivir move closer to R292 and forms two hydrogen bonds with it, while in the WT complex there is only one hydrogen bond observed between R292 and the carboxyl group of oseltamivir. The structural information is in good agreement with the free energy decomposition analysis (Figure 7c), which shows that R292 in the N294S complex has a stronger polar contribution to oseltamivir binding than that in the WT complex. The acetamide group of oseltamivir forms a hydrogen bond with R152 in the WT complex, while no hydrogen bond was found with R152 and oseltamivir in the N294S complex. The analysis based on the simulated structures is consistent with the inhibitor−protein interaction spectra.

The published works about H5N1 drug resistance suggest that the loss of the asparagine side chain at position 294 makes the main-chain carbonyl group of Y347 flip out from its position in the WT to interact with R292 and the polar hydroxyl group of the S294 residue forms a hydrogen bond with the carboxylate of E276; E276 in the N294S mutant acts as the center of the H-bond network between R224 and S294.[26,51,104] In Wang and Zheng's work, no hydrogen bond between S294 and E276 was observed, but instead, they found a salt bridge between E276 and R224, and the conformational change of E276 in H5N1 is a key source of drug resistance in the H274Y mutant but not in the N294S mutant. However, in our work, the loss of the asparagine side chain at position 294 does not make the N347 (the corresponding residue at position 347 in H5N1 NA is Tyr347) flip out from its original position in the WT NA to interact with R292, and no hydrogen bond between S294 and E276 is formed, but the salt bridge between E276 and R224 was also observed. Our results obtained from the MD simulations show that the N294S mutation influences the conformations of the R224 side chain and the $-OCHEt_2$ group, and the conformation of E276 in the N294S system changes obviously, and the mutation does not prevent the rotation of the E276 side chain. After the careful analysis of the superimposed structures, we found that the Y406 residue that can interact with the negatively charged group of oseltamivir has a relatively large conformational difference in the WT and N294S complexes (Figure 10b). Moreover, as shown in Figures 10b and 12, some residues in the active site undergo relatively large conformational change when N294 is mutated to S294. On the basis of the above analyses, we conclude that, similar to H274Y, N294S also distorts the geometry of the binding site and then impairs the interactions between oseltamivir and NA.

The Y252H Mutation. The predicted binding free energy of oseltamivir with the Y252H mutant is almost the same as that of oseltamivir with the WT NA, which is consistent with the experimental data that the Y252H mutation in H5N1 NA does not cause drug resistance to oseltamivir.[22] According to the simulated structures shown in Figure 10, it can be found that the changes in the position of oseltamivir and the adjacent side

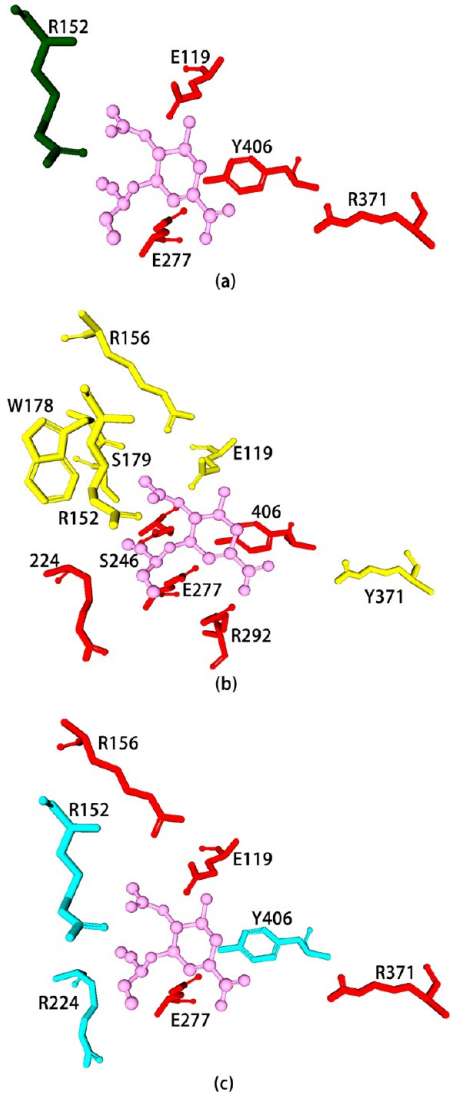

Figure 12. (a) Geometries of the five residues that contribute most to the difference between the inhibitor−residue interactions of the WT complex and those of the Y252H complex. (b) Geometries of the 11 residues that contribute most to the difference between the nonpolar (ΔG_{vdw} + ΔG_{SA}) inhibitor−residue interactions of the WT complex and those of the Y252H complex. (c) Geometries of the seven residues that contribute most to the difference between the total polar (ΔG_{ele} + ΔG_{GB}) inhibitor−residue interactions of the WT complex and those of the Y252H complex. The residues with stronger interactions with the Y252H complex are colored in red, and those with stronger interactions with the WT complex in atrovirens are colored yellow or blue. The structure of oseltamivir is shown as a pink ball-and-stick.

chains in the Y252H complex are smaller than those in the H274Y and N294S complexes, and the RMSDs for WT/H274Y, WT/N294S, and WT/Y252H are 1.71 Å, 1.58 Å, and 1.38 Å, respectively. However, the substitution of tyrosine by histidine still has an obvious impact on the conformations of oseltamivir and several adjacent residues, such as R152, E277, R371, and Y406 in the Y252H. According to the binding energy decomposition analysis shown in Table S2 and Figure 8, the contributions of E119, R152, E277, R371, and Y406 in the WT and Y252H complexes have relatively larger differences. E119, E277, R371, and Y406 form stronger interaction with oseltamivir in the Y252 complex, while R152 forms stronger interactions with oseltamivir in the WT complex. The

dx.doi.org/10.1021/ci300375k | J. Chem. Inf. Model. 2012, 52, 2715−2729

contributions of E119 and R371 are primarily dominated by the electrostatics, and the contribution of Y406 is mainly dominated by the nonpolar interaction, while the contributions of R152 and E277 are dominated by both the polar and the nonpolar interactions. Our results are significantly different from the results reported by Kar and Knecht[31] on the influenza N8 neuraminidase in that the contributions from residues E119, D151, R292, and R371 decreased significantly, leading to a significant loss of the total binding free energy. The spatial distribution of the key residues is shown in Figure 12. In summary, the Y252 mutation changes the conformation of the active site, but it does not obviously influence the binding of oseltamivir.

CONCLUSION

In the present study, a comprehensive computational strategy by combining MD simulations, MM/PBSA binding free energy calculations, and MM/GBSA binding energy decomposition analysis was used to characterize the interactions between oseltamivir and the four N1H1 neuramindases: WT NA and the three variants H274Y, N294S, and Y252H. The mechanism of drug resistance caused by the studied mutations was delineated by the energetic and structural analyses. According to the predicted binding free energies, the inhibitory potencies of oseltamivir toward the WT and mutants were predicted in the following ranked order: WT (-35.88 ± 1.13 kcal/mol) ~ Y252H (-35.39 ± 2.11 kcal/mol) > N294S (-25.21 ± 2.91 kcal/mol) > H274Y (-23.34 ± 2.64 kcal/mol). That is to say, oseltamivir would be significantly resistant to the H274Y and N294S mutants of A/H1NA NA, which is consistent with the experimental results.

The good correlation ($r^2 = 0.93$) between the polar contributions ($\Delta E_{ele} + \Delta G_{PB}$) and the binding affinities suggests that the origin of resistance is mainly from the loss of the polar interactions. Furthermore, the H274 or N294 mutation in the A/H1N1 NA can trigger an obvious structural change of the binding site, and then it impairs the interactions between oseltamivir and NA. The new structural insights obtained from this study are very important for us to gain insight into the potential drug resistance mechanism of the intermolecular interactions between oseltamivir and drug-resistant mutants.

ASSOCIATED CONTENT

Supporting Information

(Table S1) The atom types and partial charges for oseltamivir. (Table S2) Binding free energy contributions of the key binding-site residues calculated from the binding energy decomposition (kcal/mol). (Figure S1) Sequence alignment of influenza A/H1N1 NA with 3cl0 (influenza A/H5N1 NA) used for homology modeling. (Figure S2) RMSD of the active site residues (the residues within 5 Å of oseltamivir) of NA with respect to the first snapshot as a function of time (black, red, green, and blue lines represent WT, H274Y, N294S, and Y252H, respectively). (Figure S3) Fluctuations of the (a1) total nonpolar ($\Delta E_{vdw} + \Delta G_{nonpolar}$), (b1) total polar ($\Delta E_{ele} + \Delta G_{PB}$), and (c1) total binding energy (ΔG_{total}) interactions between oseltamivir and the WT NA; fluctuations of the (a2) total nonpolar ($\Delta E_{vdw} + \Delta G_{nonpolar}$), (b2) total polar ($\Delta E_{ele} + \Delta G_{PB}$), and (c2) total binding energy (ΔG_{total}) interactions between oseltamivir and the N294S NA; fluctuations of the (a3) total nonpolar ($\Delta E_{vdw} + \Delta G_{nonpolar}$), (b3) total polar ($\Delta E_{ele} + \Delta G_{PB}$), and (c3) total binding energy (ΔG_{total}) interactions between oseltamivir and the Y252H NA. (Figure S4) Inhibitor-residue interaction spectra for the WT/mutation oseltamivir complexes: (a) the total energy for the WT/oseltamivir complex, (b) the nonpolar energy ($\Delta G_{vdw} + \Delta G_{SA}$) for the WT/oseltamivir complex, and (c) the polar energy ($\Delta G_{ele} + \Delta G_{GB}$) for the WT/oseltamivir complex. (Figure S5) Inhibitor−residue interaction spectra for the WT/mutation oseltamivir complexes: (a) the total energy for the H274Y/oseltamivir complex, (b) the nonpolar energy ($\Delta G_{vdw} + \Delta G_{SA}$) for the H274Y/oseltamivir complex, and (c) the polar energy ($\Delta G_{ele} + \Delta G_{GB}$) for the H274Y/oseltamivir complex. (Figure S6) Inhibitor−residue interaction spectra for the WT/mutation oseltamivir complexes: (a) the total energy for the N294S/oseltamivir complex, (b) the nonpolar energy ($\Delta G_{vdw} + \Delta G_{SA}$) for the N294S/oseltamivir complex, (c) the polar energy ($\Delta G_{ele} + \Delta G_{GB}$) for the N294S/oseltamivir complex. (Figure S7) Inhibitor−residue interaction spectra for the WT/mutation oseltamivir complexes: (a) the total energy for the Y252H/oseltamivir complex, (b) the nonpolar energy ($\Delta G_{vdw} + \Delta G_{SA}$) for the Y252H/oseltamivir complex, (c) the polar energy ($\Delta G_{ele} + \Delta G_{GB}$) for the Y252H/oseltamivir complex. This information is available free of charge via the Internet at http://pubs.acs.org.

AUTHOR INFORMATION

Corresponding Author

*E-mail: tjhou@suda.edu.cn or tingjunhou@hotmail.com.

Present Address

Institute of Functional Nano & Soft Materials (FUNSOM), Soochow University, Suzhou 215123, P. R. China.

Notes

The authors declare no competing financial interest.

ACKNOWLEDGMENTS

This study was supported by the National Science Foundation of China (21173156), the National Basic Research Program of China (973 program, 2012CB932600), and the Priority Academic Program Development of Jiangsu Higher Education Institutions (PAPD).

REFERENCES

(1) Cheng, V. C. C.; To, K. K. W.; Tse, H.; Hung, I. F. N.; Yuen, K. Y. Two Years after Pandemic Influenza A/2009/H1N1: What Have We Learned? *Clin. Microbiol. Rev.* **2012**, *25*, 223−263.

(2) Garten, R. J.; Davis, C. T.; Russell, C. A.; Shu, B.; Lindstrom, S.; Balish, A.; Sessions, W. M.; Xu, X.; Skepner, E.; Deyde, V. Antigenic and genetic characteristics of swine-origin 2009 A (H1N1) influenza viruses circulating in humans. *Science* **2009**, *325*, 197−201.

(3) Memorandums, M. L. A revision of the system of nomenclature for influenza viruses: a WHO memorandum. *Bull. W. H. O.* **1980**, *58*, 585−591.

(4) Von Itzstein, M. The war against influenza: discovery and development of sialidase inhibitors. *Nat. Rev. Drug Discovery* **2007**, *6*, 967−974.

(5) Xu, X.; Zhu, X.; Dwek, R. A.; Stevens, J.; Wilson, I. A. Structural characterization of the 1918 influenza virus H1N1 neuraminidase. *J. Virol.* **2008**, *82*, 10493−10501.

(6) McKimm-Breschkin, J. L. Resistance of influenza viruses to neuraminidase inhibitors-a review. *Antiviral Res.* **2000**, *47*, 1−17.

(7) Kobasa, D.; Kodihalli, S.; Luo, M.; Castrucci, M. R.; Donatelli, I.; Suzuki, Y.; Suzuki, T.; Kawaoka, Y. Amino acid residues contributing to the substrate specificity of the influenza A virus neuraminidase. *J. Virol.* **1999**, *73*, 6743−6751.

(8) Cheng, L. S.; Amaro, R. E.; Xu, D.; Li, W. W.; Arzberger, P. W.; McCammon, J. A. Ensemble-based virtual screening reveals potential novel antiviral compounds for avian influenza neuraminidase. *J. Med. Chem.* **2008**, *51*, 3878−3894.
(9) Sung, J. C.; Wynsberghe, A. W. V.; Amaro, R. E.; Li, W. W.; McCammon, J. A. Role of secondary sialic acid binding sites in influenza N1 neuraminidase. *J. Am. Chem. Soc.* **2010**, *132*, 2883−2885.
(10) Amaro, R. E.; Swift, R. V.; Votapka, L.; Li, W. W.; Walker, R. C.; Bush, R. M. Mechanism of 150-cavity formation in influenza neuraminidase. *Nat. Commun.* **2011**, *2*, 388.
(11) Kolocouris, N.; Zoidis, G.; Foscolos, G. B.; Fytas, G.; Prathalingham, S. R.; Kelly, J. M.; Naesens, L.; De Clercq, E. Design and synthesis of bioactive adamantane spiro heterocycles. *Bioorg. Med. Chem. Lett.* **2007**, *17*, 4358−4362.
(12) Lew, W.; Chen, X.; Kim, C. U. Discovery and Development of GS 4104 (oseltamivir) An Orally Active Influenza Neuraminidase Inhibitor. *Curr. Med. Chem.* **2000**, *7*, 663−672.
(13) Dunn, C. J.; Goa, K. L. Zanamivir: a review of its use in influenza. *Drugs* **1999**, *58*, 761−784.
(14) Liu, H.; Yao, X.; Wang, C.; Han, J. In silico identification of the potential drug resistance sites over 2009 influenza A (H1N1) virus neuraminidase. *Mol. Pharmaceutics* **2010**, *7*, 894−904.
(15) Wang, Y. T.; Chan, C.; Su, Z. Y.; Chen, C. L. Homology modeling, docking, and molecular dynamics reveal HR1039 as a potent inhibitor of 2009 A (H1N1) influenza neuraminidase. *Biophys. Chem.* **2010**, *147*, 74−80.
(16) Yen, H. L.; Ilyushina, N. A.; Salomon, R.; Hoffmann, E.; Webster, R. G.; Govorkova, E. A. Neuraminidase inhibitor-resistant recombinant A/Vietnam/1203/04 (H5N1) influenza viruses retain their replication efficiency and pathogenicity in vitro and in vivo. *J. Virol.* **2007**, *81*, 12418−12426.
(17) de Jong, M. D.; Thanh, T. T.; Khanh, T. H.; Hien, V. M.; Smith, G. J. D.; Chau, N. V.; Cam, B. V.; Qui, P. T.; Ha, D. Q.; Guan, Y. Oseltamivir resistance during treatment of influenza A (H5N1) infection. *N. Engl. J. Med.* **2005**, *353*, 2667−2672.
(18) Lackenby, A.; Hungnes, O.; Dudman, S. G.; Meijer, A.; Paget, W. J.; Hay, A. J.; Zambon, M. C. Emergence of resistance to oseltamivir among influenza A (H1N1) viruses in Europe. *Euro-surveillance* **2008**, *13*, 1−2.
(19) Gubareva, L. V.; Kaiser, L.; Matrosovich, M. N.; Soo-Hoo, Y.; Hayden, F. G. Selection of influenza virus mutants in experimentally infected volunteers treated with oseltamivir. *J. Infect. Dis.* **2001**, *183*, 523−531.
(20) Kiso, M.; Mitamura, K.; Sakai-Tagawa, Y.; Shiraishi, K.; Kawakami, C.; Kimura, K.; Hayden, F. G.; Sugaya, N.; Kawaoka, Y. Resistant influenza A viruses in children treated with oseltamivir: descriptive study. *Lancet* **2004**, *364*, 759−765.
(21) Le, Q. M.; Kiso, M.; Someya, K.; Sakai, Y. T.; Nguyen, T. H.; Nguyen, K. H. L.; Pham, N. D.; Ngyen, H. H.; Yamada, S.; Muramoto, Y. Avian flu: isolation of drug-resistant H5N1 virus. *Nature* **2005**, *437*, 1108−1108.
(22) Collins, P. J.; Haire, L. F.; Lin, Y. P.; Liu, J.; Russell, R. J.; Walker, P. A.; Skehel, J. J.; Martin, S. R.; Hay, A. J.; Gamblin, S. J. Crystal structures of oseltamivir-resistant influenza virus neuraminidase mutants. *Nature* **2008**, *453*, 1258−1261.
(23) Pan, D.; Sun, H.; Bai, C.; Shen, Y.; Jin, N.; Liu, H.; Yao, X. Prediction of zanamivir efficiency over the possible 2009 Influenza A (H1N1) mutants by multiple molecular dynamics simulations and free energy calculations. *J. Mol. Model.* **2011**, *17*, 2465−2473.
(24) Malaisree, M.; Rungrotmongkol, T.; Decha, P.; Intharathep, P.; Aruksakunwong, O.; Hannongbua, S. Understanding of known drug-arget interactions in the catalytic pocket of neuraminidase subtype N1. *Proteins* **2008**, *71*, 1908−1918.
(25) Malaisree, M.; Rungrotmongkol, T.; Nunthaboot, N.; Aruksakunwong, O.; Intharathep, P.; Decha, P.; Sompornpisut, P.; Hannongbua, S. Source of oseltamivir resistance in avian influenza H5N1 virus with the H274Y mutation. *Amino Acids* **2009**, *37*, 725−732.
(26) Rungrotmongkol, T.; Udommaneethanakit, T.; Malaisree, M.; Nunthaboot, N.; Intharathep, P.; Sompornpisut, P.; Hannongbua, S. How does each substituent functional group of oseltamivir lose its activity against virulent H5N1 influenza mutants? *Biophys. Chem.* **2009**, *145*, 29−36.
(27) Masukawa, K. M.; Kollman, P. A.; Kuntz, I. D. Investigation of neuraminidase-substrate recognition using molecular dynamics and free energy calculations. *J. Med. Chem.* **2003**, *46*, 5628−5637.
(28) Lawrenz, M.; Baron, R.; McCammon, J. A. Independent-trajectories thermodynamic-integration free-energy changes for biomolecular systems: Determinants of H5N1 avian influenza virus neuraminidase inhibition by peramivir. *J. Chem. Theory Comput.* **2009**, *5*, 1106−1116.
(29) Shu, M.; Lin, Z.; Zhang, Y.; Wu, Y.; Mei, H.; Jiang, Y. Molecular dynamics simulation of oseltamivir resistance in neuraminidase of avian influenza H5N1 virus. *J. Mol. Model.* **2011**, *17*, 587−592.
(30) Landon, M. R.; Amaro, R. E.; Baron, R.; Ngan, C. H.; Ozonoff, D.; Andrew McCammon, J.; Vajda, S. Novel druggable hot spots in avian influenza neuraminidase H5N1 revealed by computational solvent mapping of a reduced and representative receptor ensemble. *Chem. Biol. Drug Des.* **2008**, *71*, 106−116.
(31) Kar, P.; Knecht, V. Mutation-Induced Loop Opening and Energetics for Binding of Tamiflu to Influenza N8 Neuraminidase. *J. Phys. Chem. B.* **2012**, *116*, 6137−6149.
(32) Zhang, J.; Hou, T.; Wang, W.; Liu, J. S. Detecting and understanding combinatorial mutation patterns responsible for HIV drug resistance. *Proc. Natl. Acad. Sci. U. S. A.* **2010**, *107*, 1321−1326.
(33) Amaro, R. E.; Cheng, X.; Ivanov, I.; Xu, D.; McCammon, J. A. Characterizing loop dynamics and ligand recognition in human-and avian-type influenza neuraminidases via generalized born molecular dynamics and end-point free energy calculations. *J. Am. Chem. Soc.* **2009**, *131*, 4702−4709.
(34) Amaro, R. E.; Minh, D. D. L.; Cheng, L. S.; Lindstrom, W. M., Jr; Olson, A. J.; Lin, J. H.; Li, W. W.; McCammon, J. A. Remarkable loop flexibility in avian influenza N1 and its implications for antiviral drug design. *J. Am. Chem. Soc.* **2007**, *129*, 7764−7765.
(35) Rodríguez-Barrios, F.; Balzarini, J.; Gago, F. The molecular basis of resilience to the effect of the Lys103Asn mutation in non-nucleoside HIV-1 reverse transcriptase inhibitors studied by targeted molecular dynamics simulations. *J. Am. Chem. Soc.* **2005**, *127*, 7570−7578.
(36) Hou, T.; Yu, R. Molecular dynamics and free energy studies on the wild-type and double mutant HIV-1 protease complexed with amprenavir and two amprenavir-related inhibitors: mechanism for binding and drug resistance. *J. Med. Chem.* **2007**, *50*, 1177−1188.
(37) Hou, T.; McLaughlin, W. A.; Wang, W. Evaluating the potency of HIV-1 protease drugs to combat resistance. *Proteins: Struct., Funct., Bioinf.* **2008**, *71*, 1163−1174.
(38) Chachra, R.; Rizzo, R. C. Origins of resistance conferred by the R292K neuraminidase mutation via molecular dynamics and free energy calculations. *J. Chem. Theory Comput.* **2008**, *4*, 1526−1540.
(39) Barreca, M. L.; Lee, K. W.; Chimirri, A.; Briggs, J. M. Molecular dynamics studies of the wild-type and double mutant HIV-1 integrase complexed with the 5CITEP inhibitor: mechanism for inhibition and drug resistance. *Biophys. J.* **2003**, *84*, 1450−1463.
(40) Hou, T.; Zhang, W.; Wang, J.; Wang, W. Predicting drug resistance of the HIV-1 protease using molecular interaction energy components. *Proteins: Struct., Funct., Bioinf.* **2009**, *74*, 837−846.
(41) Xue, W. W.; Qi, J.; Yang, Y.; Jin, X. J.; Liu, H. X.; Yao, X. J. Understanding the effect of drug-resistant mutations of HIV-1 intasome on raltegravir action through molecular modeling study. *Mol. Biosyst.* **2012**, *8*, 2135−2144.
(42) Xue, W. W.; Pan, D. B.; Yang, Y.; Liu, H. X.; Yao, X. J. Molecular modeling study on the resistance mechanism of HCV NS3/4A serine protease mutants R155K, A156V and D168A to TMC435. *Antiviral Res.* **2012**, *93*, 126−137.
(43) Pan, D. B.; Sun, H. J.; Shen, Y. L.; Liu, H. X.; Yao, X. J. Exploring the molecular basis of dsRNA recognition by NS1 protein of influenza A virus using molecular dynamics simulation and free energy calculation. *Antiviral Res.* **2011**, *92*, 424−433.

(44) Woods, C. J.; Malaisree, M.; Pattarapongdilok, N.; Sompornpisut, P.; Hannongbua, S.; Mulholland, A. J. Long Time Scale GPU Dynamics Reveal the Mechanism of Drug Resistance of the Dual Mutant I223R/H275Y Neuraminidase from H1N1−2009 Influenza Virus. *Biochemistry* **2012**, *51*, 4364−4375.
(45) Karthick, V.; Shanthi, V.; Rajasekaran, R.; Ramanathan, K. Exploring the Cause of Oseltamivir Resistance Against Mutant H274Y Neuraminidase by Molecular Simulation Approach. *J. Phys. Chem. B* **2012**, 1−13.
(46) Udommaneethanakit, T.; Rungrotmongkol, T.; Bren, U.; Frecer, V.; Stanislav, M. Dynamic behavior of avian influenza a virus neuraminidase subtype H5N1 in complex with oseltamivir, zanamivir, peramivir, and their phosphonate analogues. *J. Chem. Inf. Model.* **2009**, *49*, 2323−2332.
(47) Wang, N. X.; Zheng, J. J. Computational studies of H5N1 influenza virus resistance to oseltamivir. *Protein Sci.* **2009**, *18*, 707−715.
(48) Li, M. S.; Nguyen, T. T.; Mai, B. K. Study of Tamiflu Sensitivity to Variants of A/H5N1 Virus Using Different Force Fields. *J. Chem. Inf. Model.* **2011**, *51*, 2266−2276.
(49) Hitaoka, S.; Harada, M.; Yoshida, T.; Chuman, H. Correlation Analyses on Binding Affinity of Sialic Acid Analogues with Influenza Virus Neuraminidase-1 Using ab Initio MO Calculations on Their Complex Structures. *J. Chem. Inf. Model.* **2010**, *50*, 1796−1805.
(50) Park, J. W.; Jo, W. H. Infiltration of water molecules into the oseltamivir-binding site of H274Y neuraminidase mutant causes resistance to oseltamivir. *J. Chem. Inf. Model.* **2009**, *49*, 2735−2741.
(51) Rungrotmongkol, T.; Malaisree, M.; Nunthaboot, N.; Sompornpisut, P.; Hannongbua, S. Molecular prediction of oseltamivir efficiency against probable influenza A (H1N1−2009) mutants: molecular modeling approach. *Amino Acids* **2010**, *39*, 393−398.
(52) Boivin, G.; Goyette, N. Susceptibility of recent Canadian influenza A and B virus isolates to different neuraminidase inhibitors. *Antiviral Res.* **2002**, *54*, 143−147.
(53) Zürcher, T.; Yates, P. J.; Daly, J.; Sahasrabudhe, A.; Walters, M.; Dash, L.; Tisdale, M.; McKimm-Breschkin, J. L. Mutations conferring zanamivir resistance in human influenza virus N2 neuraminidases compromise virus fitness and are not stably maintained in vitro. *J. Antimicrob. Chemother.* **2006**, *58*, 723−732.
(54) Mishin, V. P.; Hayden, F. G.; Gubareva, L. V. Susceptibilities of antiviral-resistant influenza viruses to novel neuraminidase inhibitors. *Antimicrob. Agents Chemother.* **2005**, *49*, 4515−4520.
(55) Arias, C. F.; Escalera-Zamudio, M.; de los Dolores Soto-Del Río, M.; Georgina Cobián-Güemes, A.; Isa, P.; López, S. Molecular anatomy of 2009 influenza virus A (H1N1). *Arch. Med. Res.* **2009**, *40*, 643−654.
(56) McKimm-Breschkin, J. L.; Selleck, P. W.; Usman, T. B.; Johnson, M. A. Reduced sensitivity of influenza A (H5N1) to oseltamivir. *Emerg. Infect. Dis.* **2007**, *13*, 1354.
(57) Pruitt, K. D.; Tatusova, T.; Maglott, D. R. NCBI reference sequences (RefSeq): a curated non-redundant sequence database of genomes, transcripts and proteins. *Nucleic Acids Res.* **2007**, *35*, D61−D65.
(58) *Discovery Studio 2.5 Guide*; Accelrys Inc.: San Diego, CA, 2009. http://www.accelrys.com (accessed Sept. 2012).
(59) Case, D. A.; Cheatham, T. E., III; Darden, T.; Gohlke, H.; Luo, R.; Merz, K. M., Jr; Onufriev, A.; Simmerling, C.; Wang, B.; Woods, R. J. The Amber biomolecular simulation programs. *J. Comput. Chem.* **2005**, *26*, 1668−1688.
(60) Dolinsky, T. J.; Czodrowski, P.; Li, H.; Nielsen, J. E.; Jensen, J. H.; Klebe, G.; Baker, N. A. PDB2PQR: expanding and upgrading automated preparation of biomolecular structures for molecular simulations. *Nucleic Acids Res.* **2007**, *35*, W522−W525.
(61) Li, H.; Robertson, A. D.; Jensen, J. H. Very fast empirical prediction and rationalization of protein pKa values. *Proteins* **2005**, *61*, 704−721.
(62) Duan, Y.; Wu, C.; Chowdhury, S.; Lee, M. C.; Xiong, G.; Zhang, W.; Yang, R.; Cieplak, P.; Luo, R.; Lee, T. A point-charge force field for molecular mechanics simulations of proteins based on condensed-phase quantum mechanical calculations. *J. Comput. Chem.* **2003**, *24*, 1999−2012.
(63) Wang, J.; Wolf, R. M.; Caldwell, J. W.; Kollman, P. A.; Case, D. A. Development and testing of a general amber force field. *J. Comput. Chem.* **2004**, *25*, 1157−1174.
(64) Trucks, G. W.; Schlegel, H. B.; Scuseria, G. E.; Robb, M. A.; Cheeseman, J. R.; Montgomery, J. A., Jr.; Vreven, T.; Kudin, K. N.; Burant, J. C.; Millam, J. M. *Gaussian 03*, revision C. 02; Gaussian: Wallingford, CT, 2004.
(65) Bayly, C. I.; Cieplak, P.; Cornell, W.; Kollman, P. A. A well-behaved electrostatic potential based method using charge restraints for deriving atomic charges: the RESP model. *J. Phys. Chem.* **1993**, *97*, 10269−10280.
(66) Åqvist, J. Ion Water Interaction Potentials Derived from Free-Energy Perturbation Simulations. *J. Phys. Chem.* **1990**, *94*, 8021−8024.
(67) Jorgensen, W. L.; Chandrasekhar, J.; Madura, J. D.; Impey, R. W.; Klein, M. L. Comparison of simple potential functions for simulating liquid water. *J. Chem. Phys.* **1983**, *79*, 926.
(68) Berendsen, H. J. C.; Postma, J. P. M.; Van Gunsteren, W. F.; DiNola, A.; Haak, J. R. Molecular dynamics with coupling to an external bath. *J. Chem. Phys.* **1984**, *81*, 3684.
(69) Essmann, U.; Perera, L.; Berkowitz, M. L.; Darden, T.; Lee, H.; Pedersen, L. G. A smooth particle mesh Ewald method. *J. Chem. Phys.* **1995**, *103*, 8577.
(70) Ryckaert, J. P.; Ciccotti, G.; Berendsen, H. J. C. Numerical integration of the cartesian equations of motion of a system with constraints: molecular dynamics of n-alkanes. *J. Comput. Phys.* **1977**, *23*, 327−341.
(71) Miyamoto, S.; Kollman, P. A. Absolute and relative binding free energy calculations of the interaction of biotin and its analogs with streptavidin using molecular dynamics/free energy perturbation approaches. *Proteins* **1993**, *16*, 226−245.
(72) Luzhkov, V. B.; Almlöf, M.; Nervall, M.; Åqvist, J. Computational study of the binding affinity and selectivity of the bacterial ammonium transporter AmtB. *Biochemistry* **2006**, *45*, 10807−10814.
(73) Zwanzig, R. W. High-Temperature Equation of State by a Perturbation Method. I. Nonpolar Gases. *J. Chem. Phys.* **1954**, *22*, 1420−1426.
(74) Jorgensen, W. L.; Thomas, L. L. Perspective on Free-Energy Perturbation Calculations for Chemical Equilibria. *J. Chem. Theory Comput.* **2008**, *4*, 869−876.
(75) Gohlke, H.; Klebe, G. Approaches to the description and prediction of the binding affinity of small-molecule ligands to macromolecular receptors. *Angew. Chem., Int. Ed.* **2002**, *41*, 2644−2676.
(76) Kirkwood, J. G. Statistical mechanics of fluid mixtures. *J. Chem. Phys.* **1935**, *3*, 300.
(77) Srinivasan, J.; Cheatham, T. E., III; Cieplak, P.; Kollman, P. A.; David, A. Continuum solvent studies of the stability of DNA, RNA, and phosphoramidate-DNA helices. *J. Am. Chem. Soc.* **1998**, *120*, 9401−9409.
(78) Kollman, P. A.; Massova, I.; Reyes, C.; Kuhn, B.; Huo, S.; Chong, L.; Lee, M.; Lee, T.; Duan, Y.; Wang, W. Calculating structures and free energies of complex molecules: combining molecular mechanics and continuum models. *Acc. Chem. Res.* **2000**, *33*, 889−897.
(79) Wang, J. M.; Hou, T. J.; Xu, X. J. Recent advances in free energy calculations with a combination of molecular mechanics and continuum models. *Curr. Comput.-Aided Drug Des.* **2006**, *2*, 287−306.
(80) Homeyer, N.; Gohlke, H. Free Energy Calculations by the Molecular Mechanics Poisson-Boltzmann Surface Area Method. *Mol. Inf.* **2012**, *31*, 114−122.
(81) Hou, T. J.; Wang, J.; Li, Y. Y.; Wang, W. Assessing the performance of the molecular mechanics/Poisson Boltzmann surface area and molecular mechanics/generalized Born surface area methods. II. The accuracy of ranking poses generated from docking. *J. Comput. Chem.* **2011**, *32*, 866−877.
(82) Hou, T. J.; Wang, J. M.; Li, Y. Y.; Wang, W. Assessing the performance of the MM/PBSA and MM/GBSA methods. 1. The

accuracy of binding free energy calculations based on molecular dynamics simulations. *J. Chem. Inf. Model.* **2011**, *51*, 69−82.
(83) Perdih, A.; Bren, U.; Solmajer, T. Binding free energy calculations of N-sulphonyl-glutamic acid inhibitors of MurD ligase. *J. Mol. Model.* **2009**, *15*, 983−996.
(84) Lee, F. S.; Chu, Z. T.; Bolger, M. B.; Warshel, A. Calculations of antibody-antigen interactions: microscopic and semi-microscopic evaluation of the free energies of binding of phosphorylcholine analogs to McPC603. *Protein Eng.* **1992**, *5*, 215−228.
(85) Bren, U.; Lah, J.; Bren, M.; Martinek, V.; Florian, J. DNA duplex stability: the role of preorganized electrostatics. *J. Phys. Chem. B* **2010**, *114*, 2876−2885.
(86) Hou, T. J.; Zhang, W.; Xu, X. J. Binding affinities for a series of selective inhibitors of gelatinase-A using molecular dynamics with a linear interaction energy approach. *J. Phys. Chem. B* **2001**, *105*, 5304−5315.
(87) Bonnet, P.; Bryce, R. A. Molecular dynamics and free energy analysis of neuraminidase-ligand interactions. *Protein Sci.* **2004**, *13*, 946−957.
(88) Luo, R.; David, L.; Gilson, M. K. Accelerated Poisson-Boltzmann calculations for static and dynamic systems. *J. Comput. Chem.* **2002**, *23*, 1244−1253.
(89) Jedrzejas, M. J.; Singh, S.; Brouillette, W. J.; Laver, W. G.; Air, G. M.; Luo, M. Structures of aromatic inhibitors of influenza virus neuraminidase. *Biochemistry* **1995**, *34*, 3144−3151.
(90) von Itzstein, M.; Dyason, J. C.; Oliver, S. W.; White, H. F.; Wu, W. Y.; Kok, G. B.; Pegg, M. S. A study of the active site of influenza virus sialidase: an approach to the rational design of novel anti-influenza drugs. *J. Med. Chem.* **1996**, *39*, 388−391.
(91) Smith, B. J.; Colman, P. M.; Von Itzstein, M.; Danylec, B.; Varghese, J. N. Analysis of inhibitor binding in influenza virus neuraminidase. *Protein Sci.* **2001**, *10*, 689−696.
(92) Bren, U.; Martínek, V.; Florián, J. Decomposition of the solvation free energies of deoxyribonucleoside triphosphates using the free energy perturbation method. *J. Phys. Chem. B* **2006**, *110*, 12782−12788.
(93) Bren, M.; Florián, J.; Mavri, J.; Bren, U. Do all pieces make a whole? Thiele cumulants and the free energy decomposition. *Theor. Chem. Acc.* **2007**, *117*, 535−540.
(94) Hou, T.; Li, N.; Li, Y.; Wang, W. Characterization of Domain-peptide Interaction Interface: Prediction of SH3 Domain-Mediated Protein-protein Interaction Network in Yeast by Generic Structure-Based Models. *J. Proteome Res.* **2012**, *11*, 2982.
(95) Gohlke, H.; Kiel, C.; Case, D. A. Insights into protein-protein binding by binding free energy calculation and free energy decomposition for the Ras-Raf and Ras-RalGDS complexes. *J. Mol. Biol.* **2003**, *330*, 891−913.
(96) Hou, T.; Zhang, W.; Case, D. A.; Wang, W. Characterization of domain-peptide interaction interface: a case study on the amphiphysin-1 SH3 domain. *J. Mol. Biol.* **2008**, *376*, 1201−1214.
(97) Hou, T.; Xu, Z.; Zhang, W.; McLaughlin, W. A.; Case, D. A.; Xu, Y.; Wang, W. Characterization of Domain-Peptide Interaction Interface. *Mol. Cell. Proteomics* **2009**, *8*, 639−649.
(98) Hou, T. J.; Li, Y. Y.; Wang, W. Prediction of peptides binding to the PKA RII alpha subunit using a hierarchical strategy. *Bioinformatics* **2011**, *27*, 1814−1821.
(99) Onufriev, A.; Bashford, D.; David, A. Modification of the generalized Born model suitable for macromolecules. *J. Phys. Chem. B* **2000**, *104*, 3712−3720.
(100) Colman, P. M.; Varghese, J. N.; Laver, W. G. Structure of the catalytic and antigenic sites in influenza virus neuraminidase. *Nature* **1983**, *303*, 41−44.
(101) Russell, R. J.; Haire, L. F.; Stevens, D. J.; Collins, P. J.; Lin, Y. P.; Blackburn, G. M.; Hay, A. J.; Gamblin, S. J.; Skehel, J. J. The structure of H5N1 avian influenza neuraminidase suggests new opportunities for drug design. *Nature* **2006**, *443*, 45−49.
(102) Le, L.; Lee, E. H.; Hardy, D. J.; Truong, T. N.; Schulten, K. Molecular dynamics simulations suggest that electrostatic funnel directs binding of Tamiflu to influenza N1 neuraminidases. *Plos Comput. Biol.* **2010**, *6*, e1000939.
(103) Moscona, A. Oseltamivir resistance-disabling our influenza defenses. *N. Engl. J. Med.* **2005**, *353*, 2633−2636.
(104) Rungrotmongkol, T.; Intharathep, P.; Malaisree, M.; Nunthaboot, N.; Kaiyawet, N.; Sompornpisut, P.; Payungporn, S.; Poovorawan, Y.; Hannongbua, S. Susceptibility of antiviral drugs against 2009 influenza A (H1N1) virus. *Biochem. Biophys. Res. Commun.* **2009**, *385*, 390−394.
(105) Pizzorno, A.; Bouhy, X.; Abed, Y.; Boivin, G. Generation and Characterization of Recombinant Pandemic Influenza A(H1N1) Viruses Resistant to Neuraminidase Inhibitors. *J. Infect. Dis.* **2011**, *203*, 25−31.